scientific reports

Check for updates

OPEN

Naked eye detection of hydrogen peroxide via curcumin functionalised gold nanoparticles

Priya Sudhesh[1]✉, S. Sruthi[1], Mariya Jose[2], K. Vyshnavi[2], P. Aiswarya[3] & R. Manu[3]

Nanozymes are a class of inorganic nanomaterials that mimic enzyme activity. Their high durability and strong catalytic performance make them effective surrogates for natural enzymes. In this study, we synthesized curcumin-stabilized gold nanoparticles, which were employed for the colorimetric detection of hydrogen peroxide (H_2O_2) using the chromogenic substrate 3,3′,5,5′-tetramethylbenzidine (TMB). Steady-state kinetic parameters were determined by varying the substrate concentrations. When H_2O_2 was used as the substrate, the Michaelis-Menten constant (Km) and the maximum reaction rate (Vmax) were found to be 3.10×10^{-3} M and 9.27×10^{-7} M/s, respectively. For TMB, the Km and Vmax values were 0.30×10^{-3} M and 1.80×10^{-7} M/s, respectively. The lower Km value for H_2O_2 indicates a higher affinity of the nanozyme for this substrate. The electron transfer ability of the nanozyme was further confirmed by cyclic voltammetry and impedence analysis, performed by immobilizing the gold nanoparticles on the surface of an electrode. Thus, this study presents a dual-mode method for the detection of H_2O_2 using curcumin-stabilized gold nanoparticles.

Artificial enzymes, or nanozymes, are a class of inorganic materials that have been extensively studied due to their advantages over natural enzymes. Unlike natural enzymes, which suffer from drawbacks such as easy denaturation and sensitivity to pH and temperature, artificial nanomaterials can mimic the structure and function of enzymes while offering several benefits[1–3]. These advantages include high durability, reusability, broader pH tolerance, and low production cost, making them preferable in various applications. However, nanozymes often lack the biocompatibility and catalytic efficiency of natural enzymes, which has driven the search for nanomaterials that can overcome these limitations[4]. Incorporating biological agents during the synthesis of nanomaterials has been shown to reduce cytotoxicity and enhance their therapeutic potential[5].

Common enzyme-mimicking nanomaterials include metal nanoparticles, metal oxides, and carbon-based materials[6]. Materials such as CuO, Fe_3O_4, Co_3O_4, gold nanoparticles, and various carbon nanomaterials have been reported to exhibit enzyme-like activities[7–15]. For instance, Fe_3O_4 magnetic nanoparticles mimic peroxidase activity through a ping-pong catalytic mechanism, similar to that of horseradish peroxidase (HRP). Redox-active metal ion systems, including iron chalcogenides, iron phosphates, bimetallic nanoparticles, and metal oxide/chalcogenide composites, have demonstrated peroxidase-like activity due to their high surface-to-volume ratios, which facilitate substrate binding and electron transfer.

Metal-organic frameworks (MOFs) represent another important class of enzyme-mimicking materials. These are formed through the coordination of inorganic metal ions with organic ligands. Copper- and iron-based MOFs have been found to possess intrinsic peroxidase-mimicking capabilities. Recent studies have also reported multi-metallic MOFs containing multiple active sites, which show enhanced catalytic activity. Additionally, metal ion doping of MOFs has been shown to further improve enzyme-mimicking performance via Fenton-like mechanisms[8,16–24].

Hydrogen peroxide (H_2O_2) is a significant bioanalyte, and its detection is critical in clinical diagnostics, as well as in the food and cosmetic industries. In the food sector, H_2O_2 is often added to milk and milk products to inhibit microbial growth. However, excessive intake of H_2O_2 can pose serious health risks, including cancer, Alzheimer's disease, and cardiovascular disorders. Therefore, monitoring H_2O_2 concentrations is essential to ensure public health standards. Various analytical techniques have been employed for this purpose, including electrochemical methods, spectrophotometry, and fluorimetry[25,26].

Peroxidase is a natural enzyme that catalyzes the reduction of peroxides and other oxidants. Due to its substrate specificity and efficiency, peroxidase is widely used in biosensing, food processing, disease diagnosis, medicine, and wastewater treatment[27,28]. Horseradish peroxidase (HRP) is a well-known member of this enzyme family, renowned for its high sensitivity, rapid response, and low background interference. However, natural

[1]N.S.S. College Nemmara, Palakkad, Kerala, India. [2]Mercy College, Palakkad, Kerala, India. [3]Sri Vyasa N.S.S. College, Thrissur, Kerala, India. ✉email: priyaasudhesh@gmail.com

enzymes such as HRP are often unstable under varying environmental conditions, including changes in pH, temperature, and storage conditions[29]. To overcome these limitations, peroxidase-mimicking nanozymes with enhanced stability, reusability, and ease of synthesis and storage have been increasingly explored.

Among various artificial peroxidase nanozymes, gold nanoparticles (AuNPs) have gained attention due to their tunable morphology, surface functionalization capabilities, and excellent catalytic performance. AuNPs have been reported to mimic both glucose oxidase and peroxidase activities[30,31]. Nevertheless, their practical application is often limited by relatively low catalytic efficiency. Recent studies suggest that the plasmonic photocatalytic effect—arising from the localized surface plasmon resonance (LSPR) of noble metal nanoparticles—can enhance their enzyme-mimicking capabilities[32]. Upon photoexcitation, collective oscillations of conduction electrons occur on the nanoparticle surface, giving rise to LSPR. This property is exploited in various fields such as sensing, solar energy conversion, and nanomedicine[33–39]. Inspired by recent advances in LSPR-assisted photocatalysis, we aimed to investigate the role of AuNPs in enhancing peroxidase-mimicking activity.

In the present study, we synthesized curcumin-stabilized AuNPs using a green, one-pot method. These nanoparticles act as peroxidase mimics and were used for the spectrophotometric detection of H_2O_2. The reaction mechanism was further studied using cyclic voltammetry and impedence spectroscopy. Notably, the synthesis route avoids harsh chemicals, making it environmentally friendly and suitable for biological applications. Green synthesis techniques help reduce toxicity and environmental impact, leading to a lower carbon footprint compared to conventional methods.

The synthesized AuNPs were characterized using FTIR, SEM, TEM, UV–Vis spectrophotometry, Raman spectroscopy, impedance analysis, and cyclic voltammetry. The chromogenic substrate 3,3',5,5'-tetramethylbenzidine (TMB) was employed in the colorimetric assay. In the presence of H_2O_2, the peroxidase-mimicking AuNPs catalyze the oxidation of TMB to its blue-coloured oxidized form (TMB^+), which was monitored via UV–Vis spectroscopy. The kinetic parameters, including the Michaelis–Menten constant (Km) and reaction rate (Vmax), were determined using the Lineweaver–Burk plot.

Materials and methods

Chemicals and reagents

Gold(III) chloride trihydrate ($HAuCl_4{\cdot}3\ H_2O$), hydrogen peroxide (H_2O_2), and dimethyl sulfoxide (DMSO) were purchased from Merck Chemicals, India. 3,3′,5,5′-Tetramethylbenzidine (TMB) and buffer capsules of various pH were obtained from Alfa Aesar. All solutions were prepared using distilled water. Sodium carbonate (Na_2CO_3) and hydrochloric acid (HCl) were used to adjust the pH of solutions. pH paper with a range of 1–12 was used for pH verification. Curcumin was extracted from turmeric powder using ethanol as the solvent. All chemicals and reagents were used as received without further purification.

Methods

Preparation of TMB solution

A stock solution of TMB was prepared by dissolving 0.001 mg of TMB in 1 mL of DMSO. The solution was then diluted with 9 mL of citrate buffer, and the pH was adjusted to 5 using NaOH or HCl.

Extraction of curcumin

Curcumin was extracted from turmeric powder using a Soxhlet extractor with ethanol as the solvent. The turmeric powder was placed in the thimble of the Soxhlet apparatus and heated using a heating mantle. The extraction was performed for 6–10 cycles to ensure complete extraction, with the solvent maintained near its boiling point to prevent degradation of heat-sensitive compounds. The extract was then concentrated by distillation and further purified via column chromatography to obtain curcumin in its pure form.

Synthesis of curcumin-stabilized gold nanoparticles (Cur-AuNPs)

Curcumin-stabilized gold nanoparticles (Cur-AuNPs) were synthesized following the method reported by K. Sindhu et al. with slight modifications[40]. A total of 0.0046 g of purified curcumin was dissolved in 40 mL of distilled water, and the pH was adjusted to 9.5 using Na_2CO_3. The solution was transferred to a round-bottom flask, placed on a magnetic stirrer, and heated to 60 °C. Subsequently, 5 mL of a 4 mM aqueous solution of gold (III) chloride was added dropwise. A colour change from pale yellow to black and finally to burgundy red was observed within 15 min, indicating the formation of gold nanoparticles. The reaction mixture was stirred at room temperature for 2 h. After completion, the solution was allowed to cool naturally to room temperature. The resulting nanoparticles were purified by dialysis for two days to remove unreacted species and stored at 4 °C for further use.

To optimize the reaction conditions, the synthesis was carried out at various pH levels (8.0, 9.0, 9.5, and 10.0). A sharp surface plasmon resonance (SPR) peak was observed for reactions conducted at pH values between 9.0 and 10.0 (see Supplementary Information, Fig. S3).

Preparation of peroxidase-mimicking assay Cur-Au-NPs

The peroxidase-mimicking activity of curcumin-stabilized gold nanoparticles (Cur-AuNPs) was evaluated using 3,3′,5,5′-tetramethylbenzidine (TMB) as the chromogenic substrate. The assay mixture consisted of 500 µL of synthesized Cur-AuNPs, 500 µL of TMB solution, 200 µL of acetate buffer (pH 5), and 500 µL of hydrogen peroxide (H_2O_2). The reaction was monitored using UV–Visible spectroscopy. A characteristic colour change from purple to blue was observed, indicating the oxidation of TMB to its oxidized form (TMB^+).

To optimize the assay conditions, the experiment was repeated with variations in pH, TMB concentration, and H_2O_2 concentration. These investigations helped determine the optimal conditions for maximum peroxidase-mimicking activity of Cur-AuNPs.

Interference and real sample analysis

Interference studies were carried out to assess the selectivity of the assay. The assay (excluding H_2O_2) was performed in the presence of 1 mM concentrations of common interferents such as ascorbic acid, lactate, cholesterol, urea, and Fe^{2+} ions. The effect of these substances on the colorimetric response was analyzed. Additionally, real sample analysis was performed using commercially available milk samples to evaluate the practical applicability of the developed nanozyme system.

Enzyme kinetics

The peroxidase-like catalytic activity of Cur-AuNPs was further investigated by enzyme kinetic studies based on the Michaelis–Menten model. Time-scan UV–Vis spectroscopic measurements were carried out, and absorbance values were recorded over time. The experiments were conducted by varying the concentrations of H_2O_2 and TMB individually while keeping other components constant.

Initial reaction rates were calculated and plotted against substrate concentrations to generate Michaelis–Menten curves. Lineweaver–Burk plots (1/V vs. 1/[S]) were constructed to determine kinetic parameters such as the Michaelis–Menten constant (Km) and the maximum reaction velocity (Vmax). These parameters reflect the affinity of the nanozyme toward each substrate and the efficiency of the catalytic reaction.

Electrochemical study

The mechanism underlying the peroxidase-mimicking activity of Cur-AuNPs was studied using cyclic voltammetry (CV). A three-electrode system was employed, consisting of a glassy carbon electrode (GCE, diameter 3 mm) as the working electrode, a platinum wire as the counter electrode, and a saturated calomel electrode (SCE) as the reference.

The GCE was polished and modified by drop-casting a multilayer film of Cur-AuNPs onto the electrode surface, followed by air drying. CV measurements were conducted in an inert atmosphere within a potential window of + 1.2 V to – 0.4 V. The electrochemical behavior was analyzed in the presence of various concentrations of H_2O_2 to investigate the electron transfer properties and confirm the catalytic activity of the Cur-AuNP-modified electrode. Same electrode was used for impedence analysis inorder to understand the electron transfer ability of Cur-AuNP in the presence of Fe^{2+}/Fe^{3+} ions using 0.5 M NaCl as supporting electrolyte.

Results and discussions

Characterisation of Curcumin & Cur-AuGNP

Curcumin was extracted from turmeric powder using a Soxhlet extractor with ethanol as the solvent. The curcumin was separated from ethanol via distillation and further purified using column chromatography. The isolated curcumin was characterized by UV–Visible spectroscopy and Fourier Transform Infrared Spectroscopy (FTIR), as shown in Supporting Information (Fig. S1 and Fig. S2)[41,42].

The UV–Vis spectrum of pure curcumin displayed a characteristic absorption maximum at 438 nm. FTIR analysis of curcumin showed a distinct band at 1404 cm^{-1}, corresponding to olefinic C–C bending vibrations attached to the benzene ring. A peak at 1635 cm^{-1} was attributed to the carbonyl (C = O) stretching of the conjugated diketone system. The absorption at 1257 cm^{-1} was assigned to the aromatic C–O stretching, while peaks at 875 cm^{-1} and 766 cm^{-1} corresponded to out-of-plane and in-plane aromatic ring bending modes, respectively. A broad band around 3410 cm^{-1} was assigned to phenolic –OH stretching vibrations.

At basic pH, curcumin predominantly exists in anionic forms, which possess a strong reducing potential. These anionic curcumin species can effectively reduce Au^{3+} ions (from $AuCl_4^-$) to elemental gold (Au^0), facilitating the formation of curcumin-coated gold nanoparticles (Cur-AuNPs). The UV–Vis spectrum of Cur-AuNPs exhibited a surface plasmon resonance (SPR) band with a maximum absorption at 520 nm (Fig. 1), confirming the formation of gold nanoparticles. Dynamic light scattering (DLS) analysis revealed an average particle size of approximately 17 nm and a zeta potential of – 28.2 mV, indicating good colloidal stability due to electrostatic repulsion between particles. These results were consistent with Transmission Electron Microscopy (TEM) analysis, which further confirmed the uniform size and morphology of the synthesized nanoparticles. The inset of Fig. 1 shows the image of the synthesized Cur-AuNPs.

Further characterization by FTIR confirmed the successful functionalization of gold nanoparticles with curcumin. In the FTIR spectrum of Cur-AuNPs (Fig. 2a), characteristic bands were observed at 1628 cm^{-1} and 2322 cm^{-1}, corresponding to C = O stretching vibrations of the keto-enol form and symmetric CH_3 bending vibrations, respectively. A broad stretching band at 3298 cm^{-1} was attributed to O–H stretching. These spectral features confirmed the presence of curcumin moieties on the nanoparticle surface, supporting its role as both a reducing and stabilizing agent in the synthesis. The Raman spectrum of Cur–AuNPs, shown in Fig. 2b, exhibits two prominent peaks at 1362 cm^{-1} and 1532 cm^{-1}, which correspond to the C = C andC = O vibrational modes of curcumin, respectively. These bands show a noticeable shift to lower wavenumbers compared to those observed in bare curcumin (1601 cm^{-1} for C = C and 1626 cm^{-1} for C = O), indicating strong interaction between curcumin and the gold nanoparticle surface. Additionally, a distinct peak at 450 cm^{-1} is assigned to methoxy group vibrations, further confirming the presence of curcumin functional groups in the conjugated nanostructure[43,44].

Transmission electron microscopy (TEM) analysis revealed that the synthesized Cur-AuNPs were predominantly spherical with a uniform morphology and average particle diameter of approximately 15 nm. Size distribution analysis showed that over 90% of the particles fell within ± 10% of the average size, indicating a narrow distribution and high degree of monodispersity (Fig. 3). This uniformity is attributed to the high

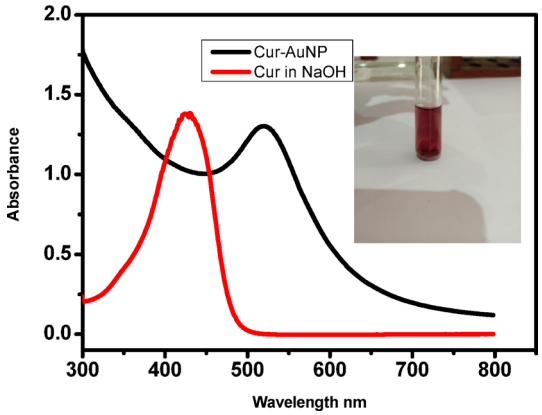

Fig. 1. UV-Vis spectra of Curcumin in NaOH and Cur-AuNP.

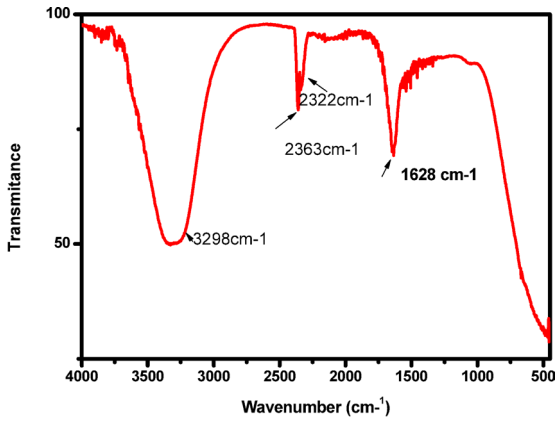

a

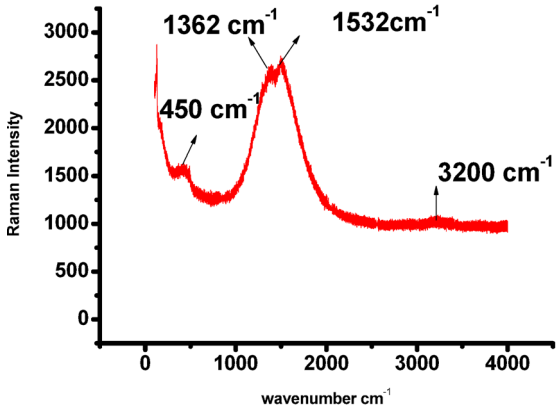

b

Fig. 2. (**a**) FTIR of Cur-AuNP, (**b**) Raman spectru of Cur-AuNP.

surface charge contributed by the hydroxyl groups in curcumin, which impart strong electrostatic repulsion and effectively prevent nanoparticle agglomeration.Selected Area Electron Diffraction (SAED) analysis was used to investigate the crystalline structure of Cur-AuNPs. The diffraction rings were indexed to the (111), (200), and (220) planes of face-centered cubic (fcc) gold. The corresponding d-spacings were calculated using ImageJ software and found to be 2.3 Å, 2.03 Å, and 1.5 Å, respectively, further confirming the crystalline nature

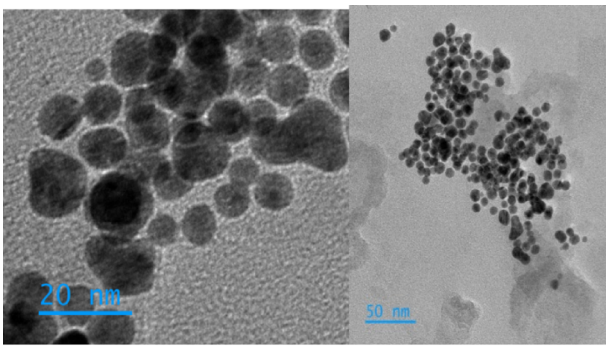

(a)

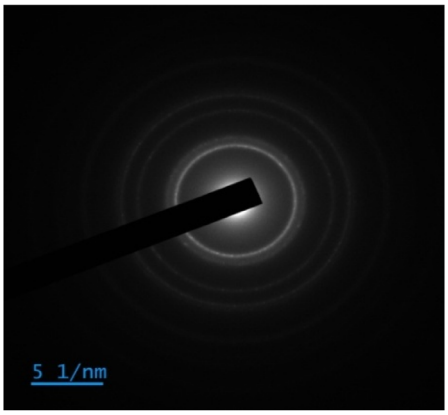

(b)

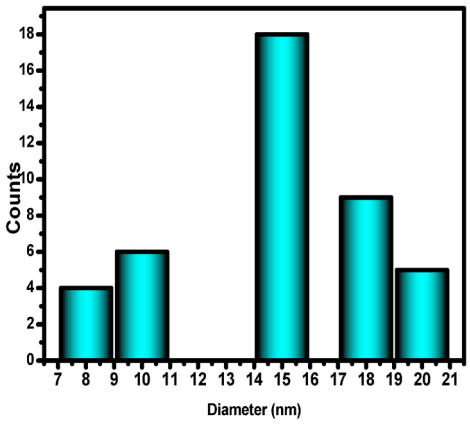

(C)

Fig. 3. (**a**) TEM image of Cur-AuNP (**b**) SAED pattern (**c**) Histogram showing size distribution.

and phase purity of the nanoparticles. Scanning electron microscopy (SEM) images (Fig. 4) corroborated the TEM findings, showing that the Cur-AuNPs were well-dispersed and spherical, with an average particle size of approximately 15 nm. The absence of significant aggregation in the SEM images also supports the role of curcumin as an effective capping and stabilizing agent.

Peroxidase mimicking property of gold nanoparticle

The peroxidase-like catalytic activity of Cur-AuNPs was evaluated using hydrogen peroxide (H_2O_2) and 3,3',5,5'-tetramethylbenzidine (TMB) as substrates in acetate buffer (pH 4). The reaction kinetics were monitored

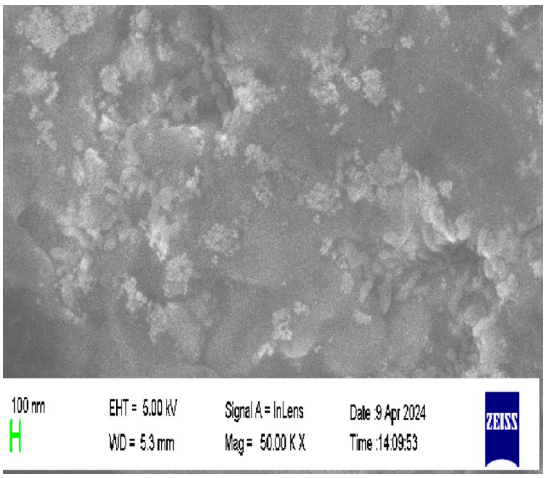

Fig. 4. SEM image of Cur-AuNP.

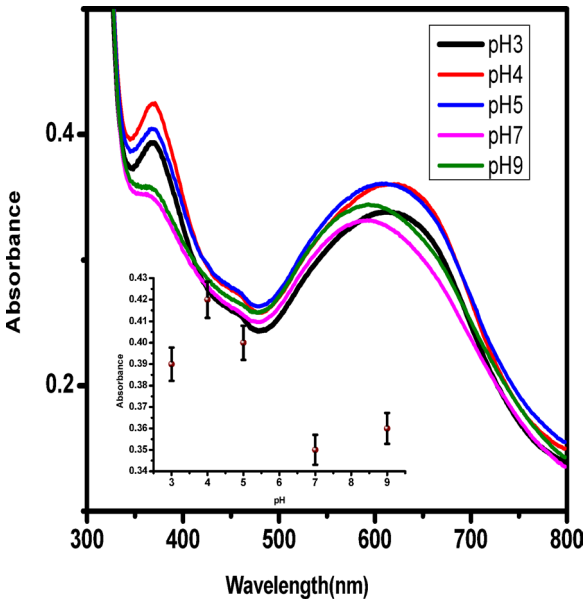

Fig. 5. Spectra of TMB oxidation under different pH conditions, Inset shows the plot intensity of absorbance against pH.

using a Thermo Scientific UV-Visible spectrophotometer in time-scan mode. In the absence of Cur-AuNPs, no oxidation of TMB was observed, even in the presence of H_2O_2, indicating that the reaction is not spontaneous and confirming the necessity of a catalyst, similar to the action mechanism of horseradish peroxidase (HRP).

TMB is a widely used chromogenic substrate for peroxidase assays. While TMB is colourless in its reduced form, its oxidized product forms a diamine charge-transfer complex, which exhibits characteristic absorption peaks at approximately 370 nm, 450 nm, and 650 nm[45–47]. The generation of a blue colour upon oxidation is indicative of peroxidase activity. To confirm the role of Cur-AuNPs in the catalytic process, a control reaction was performed using isolated curcumin (without AuNPs) with TMB and H_2O_2 under identical conditions. No observable colour change occurred, confirming that the catalytic activity arises solely from the Cur-AuNPs.

The influence of pH on peroxidase-like activity was systematically evaluated by conducting the TMB oxidation reaction at various pH values (3, 4, 5, 7, and 9) while maintaining constant concentrations of Cur-AuNPs, TMB, and H_2O_2. The catalytic activity showed a strong pH dependence, with maximum activity observed at pH 4 (Fig. 5). Therefore, pH 4 was selected as the optimal condition for all subsequent kinetic studies. Due to the overlap between the surface plasmon resonance (SPR) peak of Cur-AuNPs and the oxidized TMB peak at 650 nm, the absorbance at 370 nm was selected for time-dependent monitoring of the oxidation reaction. Additional control experiments were conducted using TMB with either Cur-AuNPs alone or H_2O_2 alone. In both cases, no characteristic absorption peak of oxidized TMB was observed, reinforcing that Cur-AuNPs facilitate the catalytic oxidation of H_2O_2 only in the presence of TMB.To assess the catalytic efficiency, kinetic studies were conducted

by varying the concentrations of either H_2O_2 or TMB, while keeping the Cur-AuNP concentration constant. The absorbance changes at 370 nm were recorded in real-time to evaluate the peroxidase-mimicking kinetics of Cur-AuNPs.

The enzyme kinetic parameters are usually calculated based on the Michaelis – Menten equation. Consider the enzyme catalytic reaction (Eq. 1)[45,46].

$$\mathbf{E} + \mathbf{S} \underset{\mathbf{k_1}}{\overset{\mathbf{k_{-1}}\,\mathbf{k_2}}{\longleftrightarrow}} \mathbf{ES} \rightarrow \mathbf{P} + \mathbf{E} \tag{1}$$

Where E is the enzyme, S is the substrate, and P is the product. Here, the enzyme (E) is replaced by enzyme mimicking material is Cur-AuNP. TMB and H_2O_2 are the substrates. The Michaelis – Menten equation for this system can be represented as

$$V = \frac{Vmax[S]}{Km + [S]} \tag{2}$$

Here V is the rate of substrate conversion, Vmax is maximum rate of substrate conversion, [S] is the concentration of the substrate, and K_m is the Michaelis – Menten constant. Thus, to study the kinetic parameters of the enzyme mimic, Cur-AuNP, Michaelis – Menten kinetics was utilized.

The peroxidase assay was performed with 500 µL of Cur-AuNP, 500µL of 1 mM TMB, 200 µL buffer and 500 µL of H_2O_2 and the absorbance changes were monitored using spectrophotometer. A peroxidase assay test was originally performed on curcumin, but no blue colour was observed. Steady-state kinetic parameters of the peroxidase mimic were carried out using different concentrations of H_2O_2 and TMB. The H_2O_2 concentration was varied from 0.5 mM to 19 mM by keeping the TMB concentration constant at 1 mM. The TMB concentration was varied from 0.05 mM to 0.5 mM by keeping the H_2O_2 concentration constant as 0.3%. The total volume of the reaction mixture was maintained at 2 mL. The concentration change of TMB was determined from time scan data using Lambert-Beer law, in which the molar absorption coefficient of oxidised TMB is taken to be $\varepsilon = 39000 M^{-1}cm^{-1}$. From the concentration term, velocity of the reaction can be obtained. The plot of velocity aganist concentration gives Michaelis-menten curves and the plot of 1/V against 1/concentration gives Lineweaver –Burk double reciprocal plot.

$$\frac{1}{\mathrm{V}} = \frac{\mathrm{Km}}{\mathrm{Vmax[S]}} + \frac{1}{\mathrm{[Vmax]}} \tag{3}$$

The kinetic parameters V_m and K_m were calculated from the Lineweaver – Burk plot. Figure 6 shows the colour change before and after the reaction. No colour change was observed in tests conducted in the presence of curcumin. This demonstrates the effectiveness of Cur-AuNP in mimicking peroxides. Figure 7 shows the time scan data. Form the plot it is clear that as concentration of H_2O_2 increases rate of reaction also increases.

Based on the experimental results, the following mechanism is proposed[48]. The catalytic reaction is initiated by the adsorption of H_2O_2 molecules onto the surface of gold nanoparticles (GNPs). Upon surface plasmon resonance (SPR) excitation, electrons and holes are generated. Due to energy alignment, the excited electrons are injected into the molecular orbitals of the adsorbed H_2O_2, promoting it to a transition state. This leads to its decomposition into a hydroxyl radical (•OH) and a hydroxide ion (OH^-).The •OH radical is a highly reactive species with a standard reduction potential of – 2.8 V and plays a key role in the rapid oxidation of TMB. Since the reaction occurs under acidic conditions, the produced OH^- ions react with H^+ ions to form water. This process suppresses the rapid recombination of electrons and holes, thereby enhancing the fission of H_2O_2 and increasing the generation of •OH radicals, ultimately accelerating the reaction rate. The proposed mechanism is illustrated in the schematic diagram. The fission of H_2O_2 was further confirmed by monitoring the absorbance

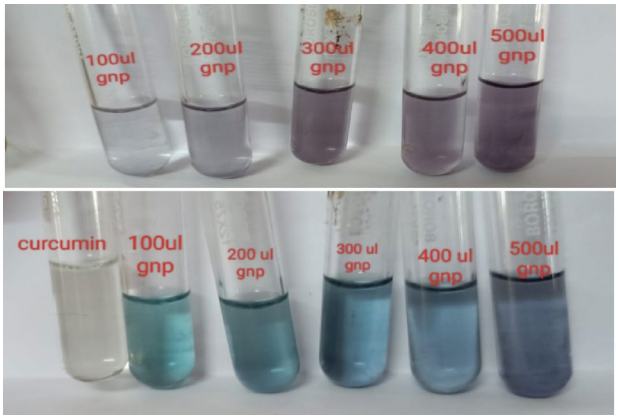

Fig. 6. Colour change observed for peroxidise mimicking assay in presence of Cur-AuNP's.

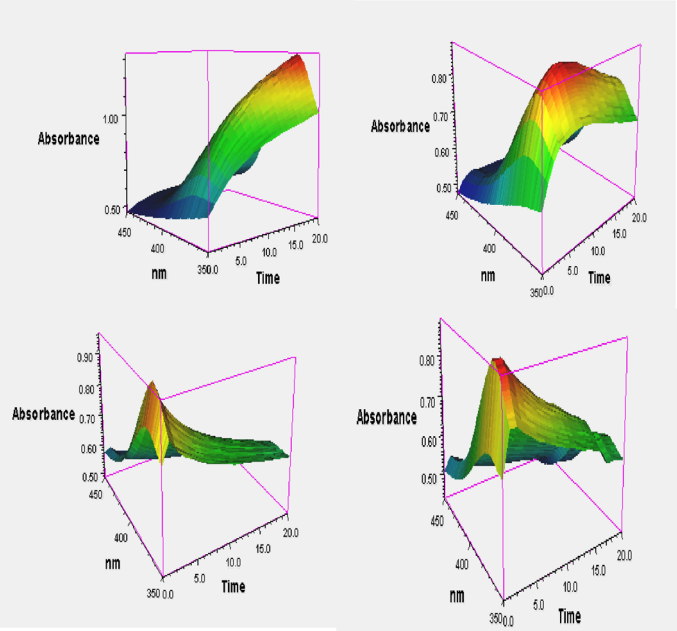

Fig. 7. Time scan data for various concentration of H_2O_2.

of H_2O_2 at 230 nm. The percentage fission ability of Cur-AuNP was compared with ascorbic acid and Curcumin (SI figure S4).

Schematic representation showing mechanism of enzyme mimic of Cur-AuNP

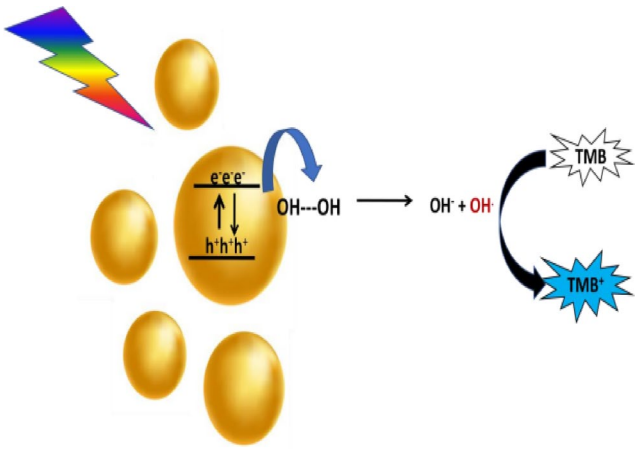

Figure 8 presents a 3D plot of absorbance versus time and wavelength for varying concentrations of H_2O_2, ranging from 0.5 mM to 19 mM. The illustration clearly demonstrates that the reaction rate increases with increasing H_2O_2 concentration. Additionally, the assay was performed using different concentrations of TMB, ranging from 0.05 mM to 0.5 mM. Figure 9a and b show the Michaelis–Menten plots for H_2O_2 and TMB substrates, respectively, while Fig. 10a and b display the corresponding Lineweaver–Burk plots. The calculated $\mathbf{K_m}$ and $\mathbf{V_{max}}$ values for H_2O_2 were 3.10×10^{-3} M and 9.27×10^{-7} M/s, respectively. For the TMB substrate, the $\mathbf{K_m}$ and $\mathbf{V_{max}}$ values were determined to be 0.3×10^{-3} M and 1.8×10^{-7} M/s, respectively. Here, $\mathbf{V_{max}}$ refers to the maximum reaction velocity, which occurs when all enzyme active sites are saturated with the substrate, and is directly proportional to the concentration of the catalyst. A comparison of the $\mathbf{K_m}$ and $\mathbf{V_{max}}$ values between the synthesized nanozyme (Cur-AuNPs) with other mimetic material and natural enzyme horseradish peroxidase (HRP) is provided in Table 1. Lower $\mathbf{K_m}$ values indicate a higher affinity of the catalyst for the substrate. According to the data, the $\mathbf{K_m}$ value for H_2O_2 is lower for Cur-AuNPs than for HRP, indicating a stronger affinity towards H_2O_2. Conversely, the $\mathbf{K_m}$ value for TMB is higher for Cur-AuNPs compared to HRP, suggesting a relatively lower affinity towards TMB.

Selectivity studies were conducted using common interfering substances, including ascorbic acid, cholesterol, dopamine, lactate, and Fe^{2+}, each at a concentration of 1 mM. No observable colour change was detected in

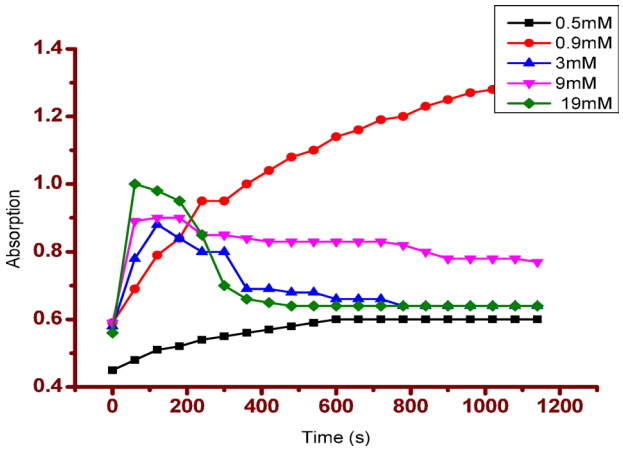

Fig. 8. Absorbance against time plot for H_2O_2 as substrate.

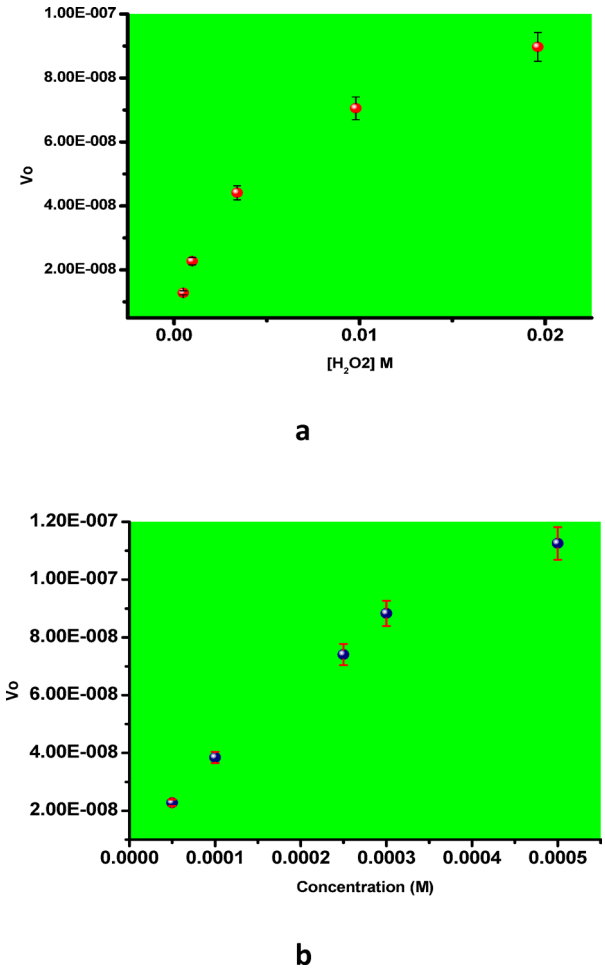

Fig. 9. (**a**) and (**b**) Michaelis –Menten plot for H_2O_2 and TMB substrates.

these tests, confirming the high selectivity of Cur-AuNPs (see SI Figure S5). The detection limit for H_2O_2 was determined to be 10 µM. Real sample analysis was performed using raw milk obtained from a local brand. The assay involved spiking known concentrations of H_2O_2 into the milk sample, followed by detection using spectrophotometry and electrochemical methods.The recovery percentage was calculated, yielding a recovery of approximately 95% (see SI Figure S6).

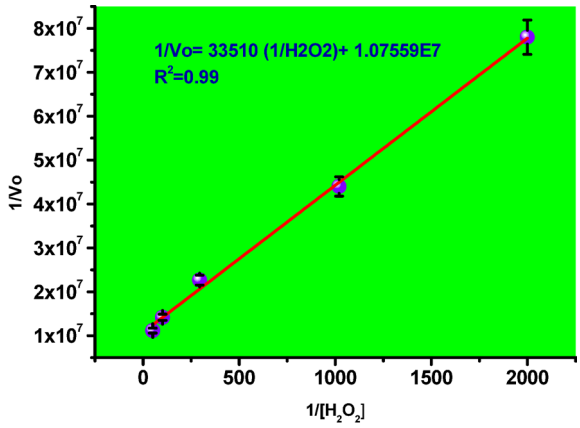

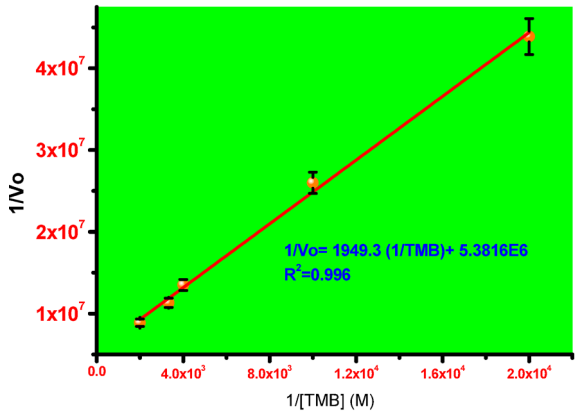

Fig. 10. (**a**) and (**b**) Lineweaver-Burk plot for H_2O_2 and TMB substrates.

Mimetic material	Substrate	Km(10^{-3})M	Vm(10^{-8})M/s
HRP[49]	TMB	0.433	10
	H_2O_2	3.72	8.7
Cu-hemin MOF[50]	TMB	1.42	26.22
	H_2O_2	2.18	116
Cu-ZIF[51]	TMB	0.22	1.31
	H_2O_2	6.7	0.91
Au-Pt nps[52]	TMB	0.42	73.2
	H_2O_2	1100	71.7
Pt NC's[53]	TMB	0.63	270
AuNS[54]	TMB	0.155	23.7
	H_2O_2	721	49
Citrate Au NP's[55]	TMB	0.134	9.65
	H_2O_2	213	10.6
Cur-Au NP's our work	TMB	0.3	18
	H_2O_2	3.1	92.7

Table 1. Comparison of kinetic parameters of Cur-AuNP with natural HRP enzyme and other enzyme mimetic materials.

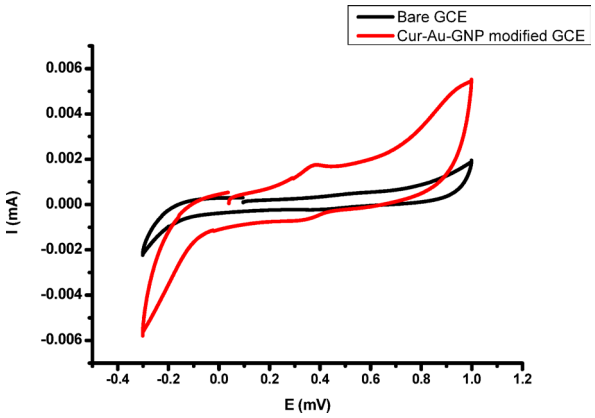

Fig. 11. Cyclic voltametric response of bare GCE and Cur-AuNP modified GCE.

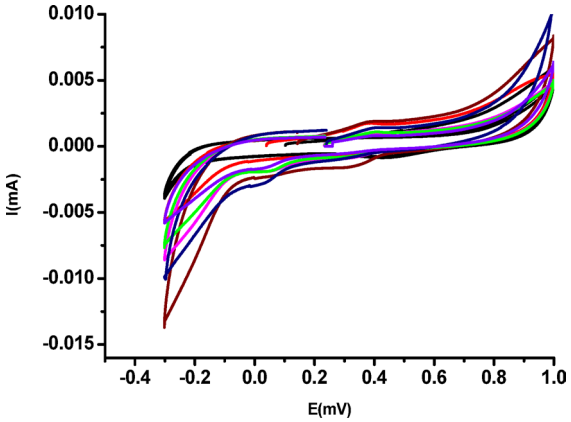

Fig. 12. Cyclic voltammetric response of Cur-AuNP modified GCE on H_2O_2 additions.

Mechanistic elucidation of H_2O_2 detection using Cur-AuNPs

To investigate the mechanism of H_2O_2 detection using Cur-AuNPs, a glassy carbon electrode (GCE) was employed. Prior to each experiment, the GCE was polished with 0.3 µm Al_2O_3 slurry, followed by thorough rinsing with methanol and Millipore water. The cleaned electrode was then immersed in phosphate buffer solution (pH 7), and cyclic voltammograms were recorded. Both bare GCE and GCE modified with Cur-AuNPs exhibited characteristic electrochemical responses in phosphate buffer (Fig. 11).The Cur-AuNP-modified GCE was subsequently used to study the electron transfer mechanism between Cur-AuNPs and H_2O_2 under nitrogen-purged conditions. Cyclic voltammetry (CV) was performed within a potential window ranging from + 1.2 V to − 0.4 V vs. SCE. The effect of H_2O_2 concentration was examined by varying the concentration from 12 µM to 87 µM (Fig. 12). A progressive increase in the cathodic current response with increasing H_2O_2 concentration was observed, indicating the catalytic activity of Cur-AuNPs in the electrochemical reduction of H_2O_2. Irreversible peaks were evident in the reverse scan, corresponding to the reduction process occurring at the Cur-AuNP-modified GCE surface.

A calibration plot of current versus H_2O_2 concentration (shown in SI Figure S7) exhibited good linearity with a correlation coefficient (R^2) of 0.98. This confirms that the AuNPs serve as effective electron-hopping centers, facilitating enhanced electron transfer at the electrode interface and thereby improving the overall electrochemical performance of the sensor. The standard redox potential (E^0) for H_2O_2 reduction vs. Hg/Hg_2Cl_2 is − 0.68 V. However, in the present system, reduction occurs at − 0.2 V, which is attributed to the catalytic effect of the Cur-AuNPs. The proposed mechanism of H_2O_2 reduction under acidic conditions is consistent with literature reports[56–60]. Table of comparison of various methods for the detection of H_2O_2 and its linear range is given in Table S1.

From the CV analysis, it is evident that Cur-AuNPs can act as efficient electrocatalysts for H_2O_2 reduction. The electron transfer ability of Cur-AuNP was further analysed with the help of impedence spectroscopy. Figure 13 shows the Nyquisit plot for bare GCE and Cur-AuGNP modified electrode in the presence of 1 mM potassium ferricyanide and potassium ferrocyanide with supporting electrolyte NaCl. Bare GCE shows linear response in lower frequency region and big semicircle at higher frequency region with an Rct value of 18821Ωcm^{-2} shows the moderate blocking nature, but after modification with Cur-AuNP the Rct value decreases to 3891 Ωcm^{-2}. This reduction in Rct values confirms the electron transfer ability of nanoparticles. Inset shows the equivalent

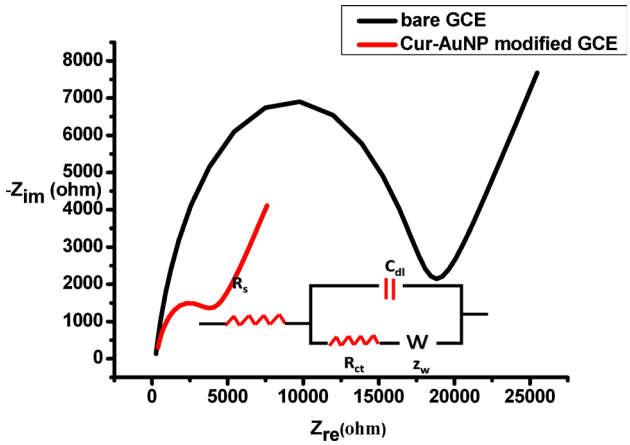

Fig. 13. Impedance plots (Nyquist plots) in equal concentrations (1 mM) of potassium ferrocyanide and potassium ferricyanide aqueous solution containing 0.1 M NaCl as supporting electrolyte. Inset shows the equivalent circuit.

circuit. This highlights their potential as peroxidase mimics, suitable for both electrochemical and colorimetric detection of H_2O_2, particularly in the presence of the chromogenic substrate TMB.

$$H_2O_2 + H^+ + e^- \longrightarrow OH_{ads} + H_2O \quad (4)$$

$$H^+OH_{ads} + e^- \longrightarrow H_2O \quad (5)$$

Conclusions

In this study, Curcumin-functionalized gold nanoparticles (Cur-AuNPs) were successfully synthesized and demonstrated excellent catalytic activity for the detection of hydrogen peroxide (H_2O_2). The proposed plasmon-enhanced mechanism involves surface adsorption of H_2O_2 and subsequent decomposition via surface plasmon resonance-induced electron excitation, leading to the formation of reactive •OH radicals. These radicals facilitate rapid oxidation of the chromogenic substrate TMB, enabling effective colorimetric detection. Kinetic analysis revealed Michaelis–Menten behavior with favorable K_m and V_{max} values, indicating a high catalytic affinity of Cur-AuNPs towards H_2O_2, surpassing that of natural horseradish peroxidase (HRP) in certain aspects. Selectivity tests confirmed minimal interference from common biological substances, while the method demonstrated a low detection limit of 10 µM and excellent recovery (~ 95%) in real sample analysis using raw milk. Electrochemical studies using Cur-AuNP-modified GCE further confirmed the catalytic role of the nanoparticles, with a significant reduction in overpotential for H_2O_2 and enhanced electron transfer efficiency. These results establish Cur-AuNPs as promising enzyme mimics for both electrochemical and colorimetric sensing platforms, with potential applications in biosensing and food safety monitoring.

Data availability

The datasets used and/or analysed during the current study available from the corresponding author on reasonable request.

Received: 16 February 2025; Accepted: 7 May 2025
Published online: 15 May 2025

References

1. Nasir, M. et al. Nanozyme-based assays for clinical diagnostics: advances and challenges. *Microchim Acta*. **184**, 323–342 (2016).
2. Wei, H. & Wang, E. Nanomaterials with enzyme-like characteristics (nanozymes): next-generation artificial enzymes. *Chem. Soc. Rev.* **42**, 6060–6093 (2013).
3. Wu, L. L., Wang, L. Y., Xie, Z. J., Xue, F. & Peng, C. F. An efficient nanozyme system based on copper nanoparticles. *RSC Adv.* **6**, 75384–75389 (2016).
4. Singh, S. Nanomaterials exhibiting enzyme-like properties (nanozymes): current advances and future perspectives. *Front. Chem.* **7**, (2019).
5. Vala, A. K. Biosynthesized silver nanoparticles and their therapeutic applications. *Biosynth. Nanomater*. **94**, 547 (2021).
6. Li, Q. et al. A high-efficiency electrocatalyst for oxidizing glucose: ultrathin nanosheet Co-based organic framework assemblies. *ACS Sustainable Chem. Eng.* **7**, 8986–8992 (2019).
7. Chen, W. et al. Nanomaterial-based enzyme mimics for biosensing applications. *ChemCatChem* **3**, 1151–1154 (2011).
8. Gao, L. et al. Intrinsic peroxidase-like activity of ferromagnetic nanoparticles. *Nat. Nanotechnol.* **2**, 577–583 (2007).
9. Mu, J., Wang, Y., Zhao, M. & Zhang, L. Intrinsic peroxidase activity of ferroferric oxide nanoparticles. *Chem. Commun.* **48**, 2540–2542 (2012).
10. Comotti, M., Pina, C. D., Matarrese, R. & Rossi, M. Aerobic oxidation of alcohols at room temperature and atmospheric pressure with gold-palladium catalysts. *Angew Chem. Int. Ed.* **43**, 5812–5815 (2004).
11. Pengo, P., Polizzi, S., Pasquato, L. & Scrimin, P. Gold nanoparticles in enzyme mimicry. *J. Am. Chem. Soc.* **127**, 1616–1617 (2005).

12. Jv, Y., Li, B. & Cao, R. Positively-charged gold nanoparticles as peroxidase mimetics and their application in hydrogen peroxide and glucose detection. *Chem. Commun.* **46**, 8017–8019 (2010).
13. Luo, W. et al. Label-free colorimetric detection of mercury ions based on peroxidase mimics of DNA–AuNPs. *ACS Nano*. **4**, 7451–7458 (2010).
14. Natalio, F. et al. Natural vanadium-dependent haloperoxidases as inspiration for new biomimetic catalysts. *Nat. Nanotechnol*. **7**, 530–535 (2012).
15. Song, Y. et al. Label-free colorimetric detection of single nucleotide polymorphism with single-base mismatch discrimination using peroxidase-like activity of graphene oxide. *Adv. Mater.* **22**, 2206–2210 (2010).
16. Tang, G., He, J., Liu, J., Yan, X. & Fan, K. Nanozyme-based diagnostics and therapeutics for infectious diseases. *Exploration* **1**, 75 (2021).
17. Lee, J. et al. Smart nanozymes: emerging strategies for theranostics. *Exploration* **2**, 20210086 (2022).
18. Wu, J. et al. Design and applications of nanozymes in biomedicine. *Chem. Soc. Rev.* **48**, 1004–1076 (2019).
19. Natalio, F. et al. Vanadium-based nanozymes mimic haloperoxidases. *Nat. Nanotechnol*. **7**, 530–535 (2012).
20. Ai, L., Li, L., Zhang, C., Fu, J. & Jiang, J. Cobalt-based frameworks for electrochemical glucose sensing. *Eur. J. Inorg. Chem*. **19**, 15105–15108 (2013).
21. Li, S. et al. 2D material-based nanozymes for biosensing. *J. Mater. Chem. B*. **11**, 7913–7919 (2023).
22. Wang, J. et al. Nanomaterials with peroxidase-mimicking activity: trends and challenges. *Anal. Chim. Acta*. **1098**, 1148–1154 (2020).
23. Yang, H. et al. Catalytic activity of metal–organic frameworks for electrochemical applications. *J. Mater. Chem*. **22**, 21849–21851 (2012).
24. Jiang, D. et al. Nanozymes: versatile platforms for diagnostics and therapeutics. *Chem. Soc. Rev.* **48**, 3683–3704 (2019).
25. Thandavan, K. et al. Zinc oxide nanowires for biosensing applications. *Sens. Actuators B*. **215**, 166–173 (2015).
26. Zhang, Y. et al. Electrochemical sensing of glucose using functionalized nanocomposites. *Int. J. Electrochem. Sci.* **15**, 8771–8785 (2020).
27. Ling, P. et al. High-performance glucose sensor based on gold nanostructures. *ACS Appl. Mater. Interfaces*. **12**, 17185–17192 (2020).
28. Liu, F. et al. Nanoparticle-based colorimetric assays for detecting disease biomarkers. *J. Nanopart. Res.* **18**, 106 (2016).
29. Vusa, K., Berchmans, S. & A., C. S. R. & Graphene oxide-gold nanocomposites for electrochemical biosensing. *Sens. Actuators B*. **253**, 723–730 (2017).
30. Lin, Y. H., Ren, J. S. & Qu, X. G. Catalytically active nanomaterials: nanozymes. *Adv. Mater.* **26**, 4200–4217 (2014).
31. Hu, Y. H. et al. Multifunctional nanozyme for biomedical applications. ACS Nano 11, 5558 – 5566 Hou, W. & Cronin, S. B. A review of surface-enhanced Raman spectroscopy of semiconductors. *Adv. Funct. Mater.* 23, 1612–1619 (2013). (2017).
32. Wang, C. L. & Astruc, D. Nanogold plasmonic catalysts: recent advances and future perspectives. *Chem. Soc. Rev.* **43**, 7188–7216 (2014).
33. Brongersma, M. L., Halas, N. J. & Nordlander, P. Plasmon-induced hot carrier science and technology. *Nat. Nanotechnol*. **10**, 25–34 (2015).
34. Linic, S., Aslam, U., Boerigter, C. & Morabito, M. Photochemical transformations on plasmonic metal nanoparticles. *Nat. Mater.* **14**, 567–576 (2015).
35. Mayer, K. M. & Hafner, J. H. Localized surface plasmon resonance sensors. *Chem. Rev.* **111**, 3828–3857 (2011).
36. Nakayama, K., Tanabe, K. & Atwater, H. A. Plasmonic nanoparticle enhanced light absorption in GaAs solar cells. *Appl. Phys. Lett.* **93**, 121904 (2008).
37. Mout, R., Moyano, D. F., Rana, S. & Rotello, V. M. Surface functionality of nanoparticles determines cellular uptake and cytotoxicity. *Chem. Soc. Rev.* **41**, 2539–2544 (2012).
38. Llevot, A. & Astruc, D. Applications of dendritic and hyperbranched polymers in catalysis. *Chem. Soc. Rev.* **41**, 242–257 (2012).
39. Sindhu, K., Rajaram, A., Sreeram, K. J. & Rajaram, R. A study on enzyme-mimicking activities of metal nanoparticles. *RSC Adv.* **4**, 1 (2014).
40. Hatcher, H., Planalp, R., Cho, J., Torti, F. M. & Torti, S. V. Curcumin: from ancient medicine to current clinical trials. *Cell. Mol. Life Sci.* **65**, 1631 (2008).
41. Teiten, M. H., Eifes, S., Dicato, M. & Diederich, M. Anti-cancer properties of Curcumin. *Toxins* **2**, 128 (2010).
42. Sindhu, K., Rajaram, A., Sreeram, K. J. & Rajaram, R. Catalytic activity of plant-derived nanoparticles. *RSC Adv.* **4**, 1808 (2014).
43. Nguyen, T. A., Tang, Q. D., Doan, D. C. T. & Dang, M. C. Micro and nano liposome vesicles containing Curcumin for a drug delivery system. *Adv. Nat. Sci. : Nanosci. Nanotechnol* **7**, (2016).
44. Shaabani, E., Amini, S. M., Kharrazi, S. & Tajerian, R. Curcumin coated gold nanoparticles: synthesis, characterization, cytotoxicity, antioxidant activity and its comparison with citrate coated gold nanoparticles. *Nanomed. J.* **4**, 115–125 (2017).
45. Veitch, N. C. Horseradish peroxidase: a modern view of a classic enzyme. *Phytochemistry* **65**, 249–259 (2004).
46. Hynninen, P. H., Kaartinen, V. & Kolehmainen, E. Structural insights into horseradish peroxidase and its biomimetic potential. *Biochim. Biophys. Acta*. **1797**, 531–542 (2010).
47. Zhang, X. Q. et al. Physicochemical properties and cytotoxicity of iron oxide nanoparticles. *J. Mater. Chem.* **20**, 5110–5116 (2010).
48. Kavya, P. et al. Thin silica shell on Ag_3PO_4 nanoparticles augments stability and photocatalytic reusability. *RSC Adv.* **13**, 30643–30648 (2023).
49. Thangavel, B., Berchmans, S. & Ganesh, V. Hollow spheres of iron oxide as an enzyme-mimic: preparation, characterization and application as biosensors. *New. J. Chem.* **46**, 4212–4225 (2022).
50. Liu, F. et al. Cu–hemin metal-organic frameworks with peroxidase-like activity as peroxidase mimics for colorimetric sensing of glucose. *J. Nanopart. Res.* **18**, 106 (2016).
51. Mechoor, A., Berchmans, S. & Venkatachalam, G. Bimetallic Cu–Zn zeolitic imidazolate frameworks as peroxidase mimics for the detection of hydrogen peroxide: electrochemical and spectrophotometric evaluation. *ACS Omega*. **8**, 39636–39650 (2023).
52. Gao, Y. C., Wang, C., Zhang, C. X., Li, H. W. & Wu, Y. Controlled Preparation and application of glutathione capped gold and platinum alloy nanoclusters with high peroxidase-like activity. *J. Mater. Sci. Technol.* **109**, 140–146 (2022).
53. Bao, Y. W., Hua, X. W., Ran, H. H., Zeng, J. & Wu, F. G. Metal-doped carbon nanoparticles with intrinsic peroxidase-like activity for colorimetric detection of H_2O_2 and glucose. *J. Mater. Chem. B*. **7**, 296–304 (2019).
54. Fernández-Lodeiro, C. et al. Synthesis of tuneable gold nanostars: the role of adenosine monophosphate. *J. Mater. Chem. C*. **11**, 12626–12636 (2023).
55. Shah, J. & Singh, S. Unveiling the role of ATP in amplification of intrinsic peroxidase-like activity of gold nanoparticles. *3Biotech* **8**, 1–12 (2018).
56. Habibi, B. & Jahanbakhshi, M. Electrochemical sensing using carbon-based nanocomposites. *J. Iran. Chem. Soc.* **12**, 1431–1438 (2015).
57. Bartlett, T. R., Holter, J., Young, N. & Compton, R. G. Nanozyme-assisted electrochemical detection. *Nanoscale* **8**, 13908–13914 (2016).
58. Mattarozzi, L. et al. Nanocomposites for electrocatalytic glucose oxidation. *Electrochim. Acta*. **198**, 296–303 (2016).
59. Niu, X. H. et al. Functional nanomaterials for hydrogen peroxide detection. *Electrochim. Acta*. **199**, 187–193 (2016).
60. Shamkhalichenar, H. & Choi, J. W. Enzyme-free biosensors based on nanomaterials. *J. Electrochem. Soc.* **164**, B3101–B3106 (2017).

Acknowledgements
Authors acknowledge CUSAT-STIC for providing instrumentation facility for characterisation. We thank Dr Sreeja Kumari, Principal Scientist NIIST, for giving valuable suggestions for TEM analysis. We also thank our parent institute for providing instrumentation facilities and support for carrying out this work.

Author contributions
P.S, S.S, V.K and M.J. wrote main manuscript and prepared figures. S.S, V.K and M.J. conducted all lab experiments. P.S reviewed the manuscript and guided the work. A.P and R.M helped in doing electrochemistry experiments.

Declarations

Competing interests
The authors declare no competing interests.

Additional information
Supplementary Information The online version contains supplementary material available at https://doi.org/10.1038/s41598-025-01613-y.

Correspondence and requests for materials should be addressed to P.S.

Reprints and permissions information is available at www.nature.com/reprints.

Publisher's note Springer Nature remains neutral with regard to jurisdictional claims in published maps and institutional affiliations.